Fe_2S_2 Protein Resonance Raman Spectra Revisited: Structural Variations among Adrenodoxin, Ferredoxin, and Red Paramagnetic Protein

Sanghwa Han,[†] Roman S. Czernuszewicz,[†] Tokuji Kimura,[‡] Michael W. W. Adams,[§] and Thomas G. Spiro*,[†]

Contribution from the Departments of Chemistry, Princeton University, Princeton, New Jersey 08544, Wayne State University, Detroit, Michigan 48202, and University of Georgia, Athens, Georgia 30602. *Received May 23, 1988*

Abstract: Resonance Raman spectra (RR) are reported for bovine adrenodoxin (Ado) and ferredoxin (Fd) from *Porphyra umbilicalis*, with ^{34}S substituted at the bridging positions of the Fe_2S_2 cluster. All of the Fe–S stretching modes are assigned on the basis of the ^{34}S isotope shifts and the previous analysis of analogue spectra. Appreciable frequency variations are seen, which can be explained on the basis of stronger Fe–S bonds, both bridging and terminal, in the proteins. This strengthening is attributable to protein compression effects or to H-bond interactions which reduced the negative charge on the iron–sulfur complex. In addition the Fe frequencies suggest an alteration in the Fe–S–C–C dihedral angles which induce mixing of the terminal Fe–S stretches with the S–C–C bending coordinate. The RR spectrum of the *Porphyra umbilicalis* Fd is identical with that of Fd isolated from *Spirulina platensis*, for which the crystal structure has been reported, as well as that of spinach Fd. RR spectra have also been obtained for a red paramagnetic protein (RPP) from *Clostridium pasteurianum*. Its frequencies suggest weakened Fe–S bridge bonding. RR spectra of reduced protein have been obtained for Ado and RPP, but not for Fd. The reduced protein spectra differ strongly from those of the oxidized proteins, and can be accounted for on the basis of a 30% reduction of the Fe–S force constants on the Fe^{II} side of the Fe_2S_2 cluster.

Among the iron–sulfur proteins,[1,2] those containing Fe_2S_2 clusters have recently commanded increasing interest. They are involved in photosynthesis,[3] hydroxylation of steroids,[4] and of camphor[5] and xanthine.[6] The terminal ligands are not limited to cysteine thiolate groups, as is now clear for the Rieske protein from *Thermus thermophilus*;[7a] a similar EPR spectrum to that of Rieske proteins has recently been reported for the Fe_2S_2 cluster of dihydroxy acid dehydratase from *Spinacea oleracea* (spinach).[7b]

The classical electron-transfer Fe_2S_2 proteins, with exclusively cysteine terminal ligands, have been divided into three classes by Meyer et al.,[8] on the basis of amino acid sequence homology. The first two classes are exemplified by the plant ferredoxins and the proteins involved in hydroxylation of organic molecules (e.g., adrenodoxin and putidaredoxin). A recently sequenced "red paramagnetic protein" (RPP) from *Clostridium pasteurianum*[8] falls in the third class.

Resonance Raman (RR) spectra of Fe_2S_2 proteins have been reported extensively.[9-19] They show modes associated with Fe–S stretching vibrations, which are enhanced via the S → Fe charge-transfer (CT) transitions which give rise to the broad absorption spectra of these proteins in the visible and near-UV.[20] The protein RR spectra show similarities, but also differences in the band positions and intensities. These differences must reflect structural variations among the proteins, but interpretation has been hampered by the absence of a thorough understanding of the nature of the modes and their dependence on structure.

A previous study from this laboratory[13] led to a number of key assignments, based on frequency shifts upon ^{34}S substitution and comparison with the RR and IR spectra of analogue complexes, supported by normal mode calculations. In the preceding paper,[21] the analysis has been extended for analogue complexes to include all of the Fe–S stretching modes, and also their coupling with S–C–C bending coordinates of bound thiolate. This analysis leads to a number of conclusions about the information provided by the protein RR spectra. These are reanalyzed in the present work for plant ferredoxin (Fd), bovine adrenodoxin (Ado), and RPP.

Experimental Section

Ferredoxins from *Porphyra umbilicalis* (red algae) and *Spinacea oleracea* (spinach) were purchased from Sigma and purified further according to the procedures described in ref 22 and 23, respectively, in order to eliminate fluorescent contaminant. Ferredoxin from *Spirulina*

Table I. Fe_2S_2 Protein RR Frequencies and $^{34}S^b$ Shifts (cm^{-1}): Assignments by Comparison with $[Fe_2S_2(S_2\text{-o-xyl})_2]^{2-}$ [a]

assign.[e]	S_2-o-xyl[a]	Ado[b]	Fd[c]	RPP[d]
B_{2u}^b	415 (6.0)[f]	421 (6.3)	426 (7.2)	408
A_g^b	391 (5.9)	393 (5.6)	395 (5.6)	387
B_{3u}^b	342 (3.2)	349 (3.2)	367 (2.0)	352
B_{1u}^t, B_{2g}^t	...[g]	341 (0.8)	357 (0.8)	
A_g^t	323 (2.0)	329 (1.5)	339 (1.2)	336
B_{1g}^b	313 (3.2)	317 (3.2)	329 (4.1)	313
B_{3u}^t	276 (3.2)	291 (3.3)	282 (3.5)	290

[a] *o*-Xylene-α,α-dithiolate analogue; data from RR and IR spectra of the tetraethylammonium salt (from ref 21). [b] Bovine adrenodoxin (oxidized). [c] *P. umbilicalis* ferredoxin (oxidized). [d] *C. pasteurianum* red paramagnetic protein (oxidized). [e] Symmetry labels for the idealized D_{2h} point group of the $Fe_2S_2^bS_4^t$ core; b = bridging and t = terminal Fe–S stretching, primarily. [f] $^{34}S^b$ isotope shifts are given in parentheses. [g] Calculated at 327 and 324 cm^{-1}, with 0 cm^{-1} $^{34}S^b$ shift; B_{2g}^t observed at 326 cm^{-1} for $[Fe_2S_2(SCH_2CH_3)_4]^{2-}$.[21]

* Author to whom correspondence should be addressed.
[†] Princeton University.
[‡] Wayne State University.
[§] University of Georgia.

(1) Thomson, A. J. In *Metalloproteins*, Part 1; Harrison, P. M., Ed.; *Topics in Molecular and Structural Biology*; Fuller, W., Neidle, S., Eds.; Macmillan: London, 1985; Chapter 3.
(2) Orme-Johnson, W. H.; Orme-Johnson, N. R. In *Iron-Sulfur Proteins*; Spiro, T. G., Ed.; Wiley-Interscience: New York, 1982; Chapter 2.
(3) Evans, M. C. W. In ref 2, Chapter 6.
(4) Estabrook, R. W.; Suzuki, K.; Mason, J. I.; Baron, J.; Taylor, W. E.; Simpson, E. R.; Purvis, J.; McCarthy, J. In *Iron-Sulfur Proteins*; Lovenberg, W., Ed.; Academic Press: New York, 1973; Chapter 8.
(5) Gunsalus, I. C.; Lipscomb, J. D. In ref 4, Chapter 6.
(6) Hille, R.; Massey, V. In *Molybdenum Enzymes*; Spiro, T. G., Ed.; Wiley-Interscience: New York, 1985; Chapter 9.
(7) (a) Cline, J. F.; Hoffman, B. M.; Mims, W. B.; LaHaie, E.; Ballou, D. P.; Fee, J. A. *J. Biol. Chem.* **1985**, *260*, 3251-3254. (b) Flint, D. H.; Emptage, M. H. *J. Biol. Chem.* **1988**, *263*, 3558-3564.
(8) Meyer, J.; Bruschi, M. H.; Bonical, J. J.; Bovier-Lapierre, G. E. *Biochemistry* **1986**, *25*, 6054-6061.
(9) Tang, S.-P. W.; Spiro, T. G.; Mukai, K.; Kimura, T. *Biochem. Biophys. Res. Commun.* **1973**, *53*, 869-874.
(10) Blum, H.; Adar, F.; Salerno, J. C.; Leigh, J. S., Jr. *Biochem. Biophys. Res. Commun.* **1977**, *77*, 650-657.
(11) Adar, F.; Blum, H.; Leigh, J. S., Jr.; Ohnishi, T.; Salerno, J.; Kimura, T. *FEBS Lett.* **1977**, *84*, 214-216.
(12) Ozaki, Y.; Nagayama, K.; Kyogoku, Y.; Hase, T.; Matsubara, H. *FEBS Lett.* **1983**, *152*, 236-240.
(13) Yachandra, V. K.; Hare, J.; Gewirth, A.; Czernuszewicz, R. S.; Kimura, T.; Holm, R. H.; Spiro, T. G. *J. Am. Chem. Soc.* **1983**, *105*, 6462-6468.

0002-7863/89/1511-3505$01.50/0

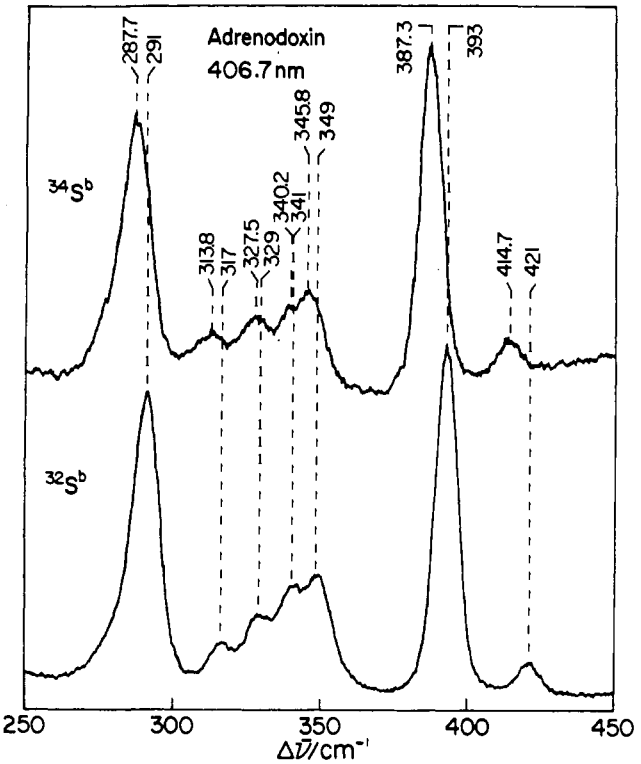

Figure 1. Resonance Raman spectra (77 K) of native and $^{34}S^{b}$-reconstituted Ado (~1 mM, pH 7.4) obtained with 406.7-nm excitation (100 mW) and 5-cm^{-1} slit widths. For these data the spectrometer was advanced in 0.2-cm^{-1} increments.

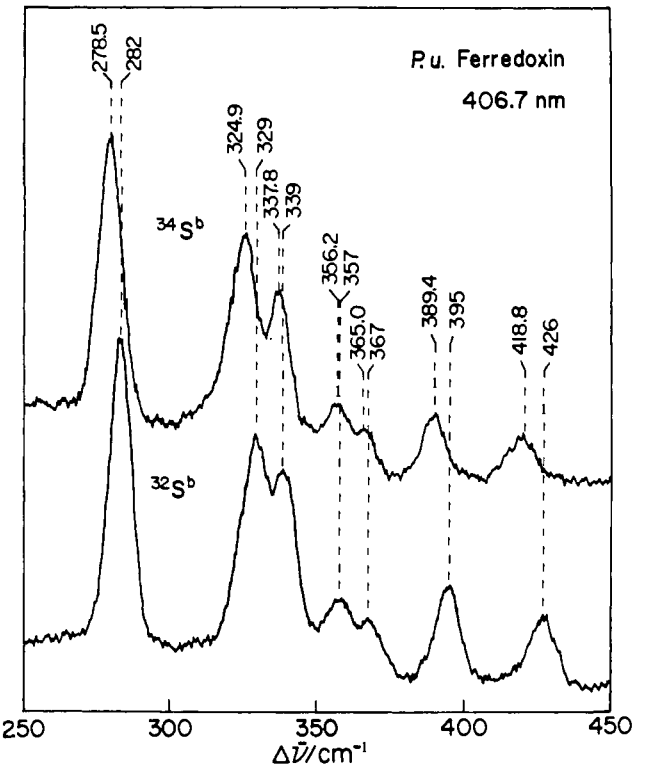

Figure 2. Resonance Raman spectra (77 K) of native and $^{34}S^{b}$-reconstituted *P. umbilicalis* Fd (~1 mM, pH 7.4); conditions as in Figure 1.

platensis (blue-green algae) was isolated[24] from commercially available lyophilized cells (Sigma). "Red paramagnetic protein" from *Clostridium pasteurianum* and adrenodoxin from bovine adrenal glands were isolated as described in ref 25 and 26, respectively. Elemental ^{34}S (95% enriched, Oakridge National Laboratories) was converted to $Na_2{}^{34}S$ by reaction with sodium metal in liquid ammonia solution,[27] and used for the reconstitution of *P. umbilicalis* Fd[28] and Ado.[29] Reconstitution of RPP with ^{34}S was not successful, however. Reduced protein samples were prepared by adding a small excess of sodium dithionite anaerobically in a glove box. For D_2O experiments the proteins were lyophilized and redissolved in buffer made up with D_2O. Good quality resonance Raman spectra were obtained via backscattering from the surface of a frozen solution (~1 mM) kept in a liquid nitrogen Dewar.[30] The spectra reported here are the accumulation of 6–10 scans with 100–150-mW laser power, and are unsmoothed. The spectrometer was advanced in 0.5-cm^{-1}/s increments; in some cases, 0.2-cm^{-1}/s increments were used for the accurate determination of isotope shifts. Other experimental details are described in the preceding paper.[21]

Results and Discussion

1. Vibrational Assignments. Figures 1 and 2 show RR spectra of bovine Ado and *P. umbilicalis* Fd in the native state and reconstituted with ^{34}S in the bridging positions. These spectra, obtained on frozen solutions, are of much better quality than those reported previously from this laboratory for Ado and spinach Fd[13] and are similar to those recently reported by Mino et al.[19] The band frequencies are nevertheless in quite good agreement, although the doublets at 341/349 cm^{-1} in Ado and 357/367 cm^{-1} in Fd were not resolved in the earlier spectra, and a spurious band at 372 cm^{-1} in adrenodoxin was reported. The frequencies and isotope shifts are listed in Table I. Assignments to the bridging and terminal Fe–S stretches are readily made by comparison with the mode assignments for the $[Fe_2S_2(S_2\text{-}o\text{-xyl})_2]^{2-}$ (S_2-*o*-xyl = *o*-xylene-α,α'-dithiolate) analogue, analyzed in the preceding study.[21] We caution again that the labels indicate the primary internal coordinate contributors to the modes, but do not reflect the substantial coordinate mixing that occurs in some of them.[21] The D_{2h} symmetry labels are only approximate, since the symmetry is lowered at least to C_{2h} by the methylene groups of the cysteine ligands, and there are other symmetry lowering influences in the vicinity of the cluster.

The isotope shifts are very similar for the proteins and the analogue, and make the correlations straightforward. There is no evidence for scrambling of the frequency order in either protein, as was earlier suggested for Ado.[13] There are nevertheless appreciable frequency differences among the three species, which are considered in the next section. The only ambiguity is the

(14) Meyer, J.; Moulis, J.-M.; Lutz, M. *Biochem. Biophys. Res. Commun.* **1984**, *119*, 828–835.
(15) Willis, L. J.; Loehr, T. M. *Biochemistry* **1985**, *24*, 2768–2772.
(16) Meyer, J.; Moulis, J.-M.; Lutz, M. *Biochim. Biophys. Acta* **1986**, *871*, 243–249.
(17) Meyer, J.; Moulis, J.-M.; Lutz, M. *Biochim. Biophys. Acta* **1986**, *873*, 108–118.
(18) Kuila, D.; Fee, J. A.; Schoonover, J. R.; Woodruff, W. H.; Batie, C. J.; Ballou, D. P. *J. Am. Chem. Soc.* **1987**, *109*, 1559–1561.
(19) Mino, Y.; Loehr, T. M.; Wada, K.; Matsubara, H.; Sanders-Loehr, J. *Biochemistry* **1987**, *26*, 8059–8065.
(20) (a) Noodleman, L.; Baerends, E. J. *J. Am. Chem. Soc.* **1984**, *106*, 2316–2327. (b) Noodleman, L.; Norman, J. G., Jr.; Osborne, J. H.; Aizman, A.; Case, D. A. *J. Am. Chem. Soc.* **1985**, *107*, 3418–3426. (c) Noodleman, L.; Case, D. A.; Aizman, A. *J. Am. Chem. Soc.* **1988**, *110*, 1001–1005.
(21) Han, S.; Czernuszewicz, R. S.; Spiro, T. G. *J. Am. Chem. Soc.* preceding paper in this issue.
(22) (a) Andrew, P. W.; Rogers, L. J.; Bouter, D.; Haslett, B. G. *Eur. J. Biochem.* **1976**, *69*, 243–248. (b) Takruri, I.; Haslett, B. G.; Boulter, D.; Andrew, P. W.; Rogers, L. J. *Biochem. J.* **1978**, *173*, 459–466.
(23) Petering, D. M.; Palmer, G. *Arch. Biochem. Biophys.* **1970**, *141*, 456–464.
(24) Hall, D. O.; Rao, K. K.; Cammack, R. *Biochem. Biophys. Res. Commun.* **1972**, *47*, 798–802.
(25) Cardenas, J.; Mortenson, L. E.; Yock, D. C. *Biochim. Biophys. Acta* **1975**, *434*, 244–257.
(26) Mukai, K.; Huang, J. J.; Kimura, T. *Biochim. Biophys. Acta* **1974**, *336*, 427–436.
(27) Brauer, G. *Handbook of Preparative Inorganic Chemistry*; Academic Press: New York, 1963; Vol. 1, pp 358–360.
(28) Rao, K. K.; Cammack, R.; Hall, D. O.; Johnson, C. E. *Biochem. J.* **1971**, *122*, 257–265.
(29) Suhara, K.; Kanayama, K.; Tekemori, S.; Katagiri, M. *Biochim. Biophys. Acta* **1974**, *336*, 309–317.
(30) Czernuszewicz, R. S.; Johnson, M. K. *Appl. Spectrosc.* **1983**, *37*, 297–298.

Table II. Illustrative Normal Mode Calculations (cm^{-1}) for Fe_2S_2 Species

	S_2-o-xyl[a]		Ado[b]		Ado-(S_2-o-xyl)		Fd[c]		Fd–Ado	
mode	obs	calc	obs	calc	obs	calc	obs	calc	obs	calc
$B_{2u}{}^b$	415	414	421	419	6	5	426	423	5	4
$A_g{}^b$	391	392	393	394	2	2	395	400	2	6
$B_{3u}{}^b$	342	340	349	350	7	10	367	361	18	11
$B_{1u}{}^t$,$B_{2g}{}^t$		327	341	335	14	7	357	349	16	14
$A_g{}^t$	323	323	329	327	6	4	339	339	10	12
$B_{1g}{}^b$	313	311	317	316	4	5	329	318	12	2
$B_{3u}{}^t$	276	275	291	283	15	8	282	279	−9	−4

[a] *o*-Xylene-α,α-dithiolate analogue; see ref 21 for force constants. [b] Bovine adrenodoxin; the same geometry and force field as S_2-o-xyl except $K(Fe-S^b)$ raised from 1.31 to 1.40 mdyn/Å and $K(Fe-S^t)$ raised from 1.14 to 1.20 mdyn/Å. [c] *P. umbilicalis* ferredoxin; Fe–S–C–C dihedral angle increased from 90 to 105°; the same force field as S_2-o-xyl except $K(Fe-S^b)$ and $K(Fe-S^t)$ raised to 1.43 and 1.28 mdyn/Å.

assignment of the band at 341 cm^{-1} in Ado and 357 cm^{-1} in Fd. This corresponds to either or both of the $B_{2g}{}^t$ and $B_{1u}{}^t$ modes. These terminal stretches are accidentally degenerate in the analogue spectra because they differ only in the phasing of the stretches on opposite sides of the Fe_2S_2 bridge.[21] One is Raman-active and the other infrared-active. Since infrared modes are activated in the protein RR spectra, due to symmetry lowering (see next section), either mode (or both) could be responsible for the protein bands. The $^{34}S^b$ shifts of the protein bands, 0.8 cm^{-1}, are probably artifacts of the larger shifts of the nearby 349- and 367-cm^{-1} bands, since zero shifts are expected for these purely terminal modes.[21]

Also listed in Table I are the observed frequencies for *C. pasteurianum* RPP (see Figure 8). While ^{34}S reconstitution was unsuccessful for this protein, the frequency correspondences leave little doubt about the assignments in this case as well.

A point of interest is that an extra band attributable to S–C–C bending is not seen in the protein spectra. For the analogue this band is found at 306 cm^{-1}, adjacent to the $B_{1g}{}^b$ band at 313 cm^{-1}, whose isotope shift it shares.[21] It is this near-degeneracy and the resultant mode mixing which produce the S–C–C bend activation; deuteration of the xylenedithiolate methylene groups, adjacent to the terminal S atoms, shifted the S–C–C bending frequency sufficiently to unmix the modes, leading to the disappearance of the S–C–C bend. At the same time the $B_{1g}{}^b$ $^{34}S^b$ isotope shift increased from 3.2 to 4.8 cm^{-1} due to the unmixing of the modes.[21] For Fd, the $B_{1g}{}^b$ mode shifts up to 329 cm^{-1} and the $^{34}S^b$ shift is 4.1 cm^{-1}, consistent with only weak mixing with the S–C–C bending mode, whose intensity should therefore be low. For Ado and RPP the $B_{1g}{}^b$ frequencies, 317 and 313 cm^{-1}, are close to those of the analogue, as is the $^{34}S^b$ shift for Ado, so that substantial mixing with S–C–C bending is expected. The $B_{1g}{}^b$ band intensities are weak for Ado and RPP, however, and the S–C–C bending mode may escape detection for this reason.

2. Force Constant and Conformational Differences. We now consider likely sources of the frequency variation in the Fe–S stretching modes. The xylenedithiolate analogue frequencies and isotope shifts have been calculated with a physically reasonable modified Urey–Bradley force field.[21] The observed and calculated frequencies are reproduced in Table II and compared with the protein data. The Ado frequencies are higher than the xylenedithiolate analogue frequencies by 2–15 cm^{-1}. Table II shows that the Ado frequencies can be calculated reasonably well with the xylenedithiolate analogue structural model and a force field which is altered only by raising the principal force constants for bridging and terminal Fe–S stretching by 2 and 5%. Five of the seven frequencies are calculated to within experimental error, while two of them, $B_{1u}{}^t$ and $B_{3u}{}^t$ are 7 cm^{-1} higher than calculated. These deviations could be corrected by small changes in the nonbonded or valence interaction force constants.

It seems clear that the Ado spectrum can be explained on the basis of the xylenedithiolate analogue spectrum provided that the Fe–S bonds are strengthened slightly in the protein. Possible sources of Fe–S bond strengthening include compression effects of the protein tertiary structure and H-bonding to the S atoms from nearby donor groups in the protein. Such H-bonding is a theme in all Fe–S protein crystal structures so far reported, including that of *S. platensis* Fd.[31] Mino et al.[19] have recently shown that these H bonds are strong enough to permit detectable perturbation of the Fe–S stretching RR frequencies when Fe_2S_2 proteins are equilibrated with D_2O.[32] The effect of H-bonding on the Fe–S bond strengths is difficult to predict. By removing electron density from the S atoms, the H bonds should reduce the donor strength of the sulfide and thiolate ligands, but at the same time relief of the overall negative charge of the $Fe_2S_2{}^bS_4{}^t$ complex, formally 2- in the oxidized state, may increase the Fe–S bond strength by diminishing the S···S repulsions. Whether protein mechanical forces or H-bonding (or both) are responsible for the effects is not clear. The Ado results suggest that both bridging and terminal bonds are strengthened about equally.

When Fd is compared with Ado (Table II), a different pattern of variation is noted. Strong upshifts are seen for the group of bands between 320 and 370 cm^{-1}, while the lowest frequency band, $B_{3u}{}^t$, shifts *down*. This is just the pattern expected if the Fe–S–C–C dihedral angles are increased from the 90° value used in the xylenedithiolate analogue calculation. This variation was analyzed in the preceding paper.[21] Mixing of the Fe–S stretches with the S–C–C bending coordinate, whose natural frequency is ~300 cm^{-1}, depends strongly on the Fe–S–C–C dihedral angle. It is minimized at 90°, where the Fe–S stretching and S–C–C bending coordinates are orthogonal, and maximized at 180° where they are in line. Because the natural frequency of S–C–C bending is near 300 cm^{-1}, the modes above 300 cm^{-1} increase with increasing dihedral angle, while the one mode below 300 cm^{-1}, $B_{3u}{}^t$, decreases. The results in Table II show that the Fd frequencies can be calculated reasonably well starting with the xylenedithiolate model if the bridging and terminal Fe–S stretching force constants are allowed to increase still further while the Fe–S–C–C dihedral angles are increased from 90 to 105°. Again five of the seven frequencies are calculated to within experimental error. The requirement for dihedral angles greater than 90° is implied qualitatively by the large gap between the $B_{3u}{}^t$ mode and the group of bands between 325 and 370 cm^{-1}. It is unrealistic, however, to expect the four Fe–S–C–C dihedral angles to change uniformly from one protein to another. These angles have not been reported for the *S. platensis* Fd crystal structure, but visual inspection of the published model[33] suggests that two of the angles are near 90° while the other two are closer to 180°. Trial calculations indicate that the frequencies change progressively, but not monotonically, when the four Fe–S–C–C dihedral angles are increased two at a time. A distribution of dihedral angles could account for some of the deviations between observed and calculated frequencies in Table II.

Table III compares structural parameters from the *S. platensis* Fd crystal structure[33,34] with those of the xylenedithiolate ana-

(31) (a) Stout, C. D. In *Iron-Sulfur Proteins*; Spiro, T. G., Ed.; Wiley-Interscience: New York, 1982; Chapter 3. (b) Tsukihara, T.; Fukuyama, K.; Katsube, Y. In *Iron-Sulfur Protein Research*; Matsubara, H., Katsube, Y., Wada, K., Eds.; Springer-Verlag: West Berlin, 1986; pp 59–69.

(32) The equilibration is slow, taking at least 4 days at 5 °C.[19] In our hands no RR spectral changes were observed upon redissolving the lyophilized protein in D_2O buffer.

(33) Tsukihara, T.; Fukuyama, K.; Nakamura, M.; Katsube, Y.; Tanaka, N.; Kakudo, M.; Wada, K.; Matsubara, H. *J. Biochem. (Tokyo)* **1981**, *90*, 1763–1773.

(34) Tsukihara, T., unpublished data cited in ref 31a, Table 7.

Table III. Comparison of Structural Parameters for $(Et_4N)_2[Fe_2S_2(S_2\text{-o-xyl})_2]$ and Ferredoxin from *S. platensis*.[a]

	S_2-o-xyl[b]	Fd[c]
	Distance (Å)	
Fe–S^b	2.209	2.01
Fe–S^t	2.305	2.23
Fe···Fe	2.698	2.72
S^b···S^b	3.498	2.94
S^b···S^t	3.730	3.54
S^t···S^t	3.690	3.44
	Angles (deg)	
Fe–S^b–Fe	75.3	86
S^b–Fe–S^b	104.7	89
S^t–Fe–S^t	106.4	101

[a] Average of equivalent bonded (–) and nonbonded (···) distances, and angles. [b] $(Et_4N)_2[Fe_2S_2(S_2\text{-o-xyl})_2]$ analogue (data from ref 35). [c] *S. platensis* ferredoxin (data from ref 33). Unusually long Fe–S(Cys41) bond was excluded from the calculation.

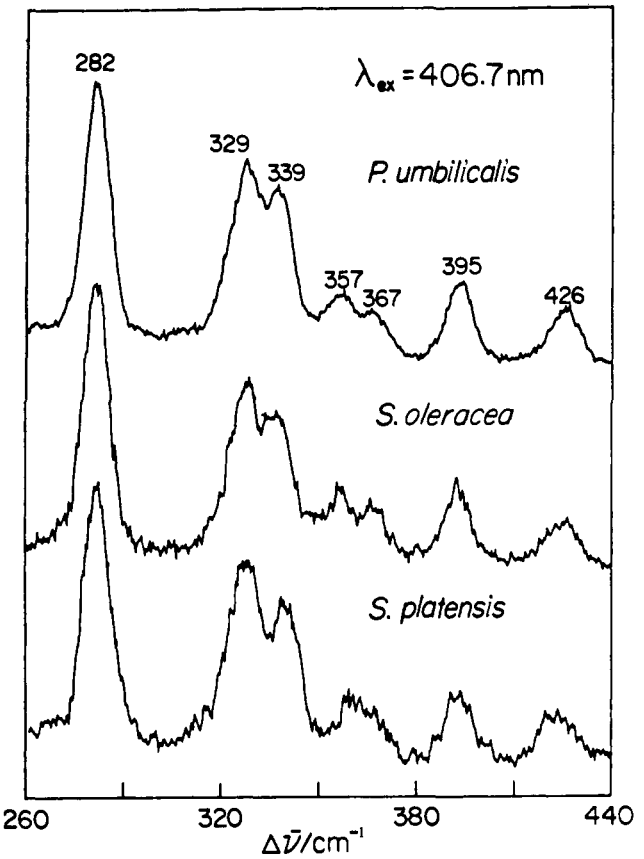

Figure 3. Resonance Raman spectra (77 K) of three plant-type Fd's from *P. umbilicalis* (red algae), *S. oleracea* (spinach), and *S. platensis* (blue-green alga). Conditions as in Figure 1, with the exception that the spectrometer was advanced in 0.5-cm^{-1} increments.

logue.[35] The protein determination is, of course, at much lower resolution than is that of the analogue, and the quantitative significance of the reported differences is uncertain. However, there is an apparent contraction of the entire complex, with a shortening of both Fe–S^b and Fe–S^t bonds, qualitatively consistent with the vibrational data.

Figure 3 shows that the RR spectrum of Fd from *P. umbilicalis*, *S. platensis*, and spinach (*S. oleracea*) are essentially the same so that the *S. platensis* crystal structure is clearly relevant to the spectral analysis. On the other hand Mino et al.,[19] who pointed out the close similarity of RR spectra of Fd from spinach and from *S. platensis*, nevertheless, found that frequency shifts induced by D_2O are greater for the former than for the latter (e.g., 0.8 versus 0.5 cm^{-1} for the ~390-cm^{-1} band) suggesting that there are structural differences sufficient to alter the H-bond strengths.

(35) Mayerle, J. J.; Denmark, S. E.; DePamphilis, B. V.; Ibers, J. A.; Holm, R. H. *J. Am. Chem. Chem. Soc.* **1975**, *97*, 1032–1045.

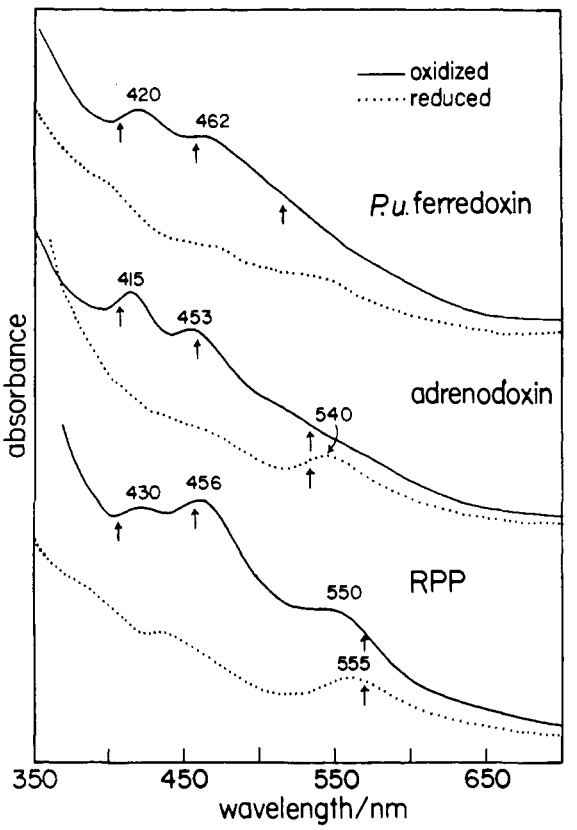

Figure 4. Electronic absorption spectra at room temperature of oxidized (solid line) and reduced (dotted line) *P. umbilicalis* (P.u.) Fd, bovine Ado, and *C. pasteurianum* RPP at pH 7.4. Arrows mark the Raman excitation wavelengths.

The RPP spectrum (Table I and Figure 8) is different from that of either Ado or Fd. We have not attempted to model its frequencies, but we note that the gap between $A_g{}^t$ and $B_{3u}{}^t$ is similar to that in Ado, suggesting that the Fe–S–C–C dihedral angles are not far from 90°. The high-frequency bridging modes $B_{2u}{}^b$ and $A_g{}^b$ are lower in frequency than the xylenedithiolate analogue, in contrast to Ado and Fd. This suggests that the bridge bonds are weakened slightly.

3. Intensities and Wavelength Dependence. Figure 4 shows absorption spectra of *P. umbilicalis* Fd, bovine Ado, and *C. pasteurianum* RPP in oxidized and reduced forms. The complex features throughout the visible and near-UV region are attributable to S → Fe^{III} charge-transfer (CT) transitions. Theoretical electronic calculations by Noodleman et al.[20] indicate a series of overlapping CT transitions involving both bridging and terminal ligands. We have measured excitation profiles (EP's) for Ado, as shown in Figure 5, with the available lines from Kr^+ and Ar^+ lasers. These profiles roughly track the absorption spectrum, showing increasing Raman intensity with decreasing wavelength, the largest cross sections being obtained at 413.1 nm, in resonance with the 415-nm absorption band. At least five peaks can be seen in the EP's, and more are likely between 550 and 650 nm. Because of the likelihood of interference effects among the scattering contributions from the different CT transitions, the wavelengths of the EP maxima are not necessarily the same as those of the CT transitions themselves. Although the different RR bands show different relative cross sections in the various EP peaks, there is not a clear sorting into bridging and terminal enhancement patterns. Thus significant bridging as well as terminal involvement in most of the CT transitions seems likely.

A view of the wavelength selectively for the various Raman bands is given in Figures 6, 7, and 8, which show RR spectra for *P. umbilicalis* Fd, bovine Ado, and *C. pasteurianum* RPP, respectively, at three different wavelengths, in the violet, blue, and

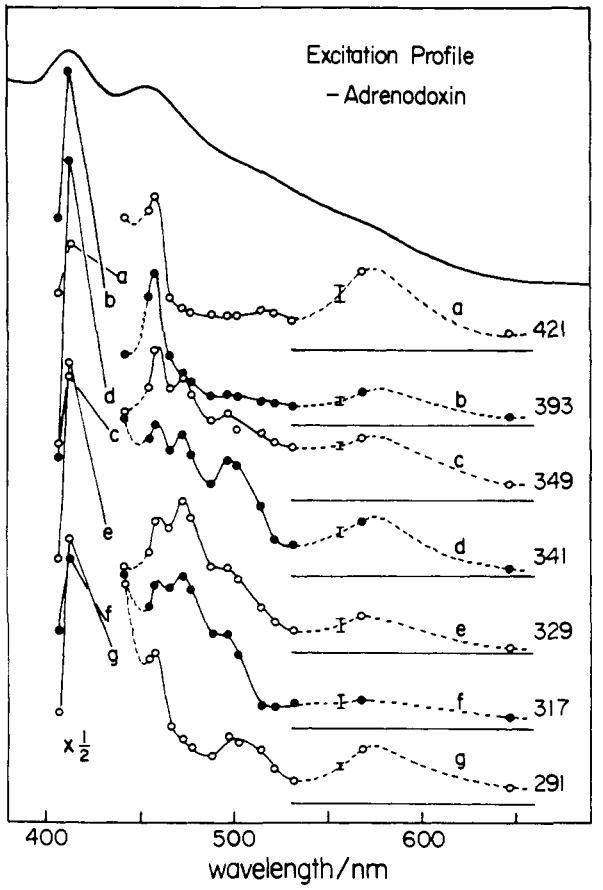

Figure 5. Raman excitation profiles for the indicated bands (cm^{-1}) of Ado at 77 K. The ice band at ~225 cm^{-1} served as an internal standard (see Figure 7) and representative error bars are marked on the figure.

Table IV. Observed Overtone and Combination Frequencies (cm^{-1}) for Fe_2S_2 Proteins

assignments[a]	Ado[b]	Fd[c]	RPP[d]
$2 \times B_{3u}{}^t$	581	563	578
$B_{3u}{}^t + A_g{}^t$		622	
$B_{3u}{}^t + B_{3u}{}^b$	641	650	641
$2 \times A_g{}^t$		675	675
$B_{3u}{}^t + A_g{}^b$	683		
$B_{3u}{}^b + A_g{}^b$	741	760	736
$2 \times A_g{}^b$	786	794	774

[a] See Table I. [b] Bovine adrenodoxin. [c] *P. umbilicalis* ferredoxin (oxidized). [d] *C. pasteurianum* red paramagnetic protein (oxidized).

green or yellow region. These spectra show considerable variation in the enhancement pattern for the three proteins. For example, Fd shows maximal enhancement of the 395-cm^{-1} $A_g{}^b$ bridge breathing mode at 457.9 nm, while for Ado and RPP, maximal enhancement of this mode is seen in the violet (406.7 nm) and the yellow (568.2 nm) region, respectively. Thus the bridge breathing mode enhancement responds quite differently to the CT transitions of the three proteins. On the basis of the idealized D_{2h} geometry of the $Fe_2S_2{}^bS_4{}^t$ complex, the two totally symmetric modes, $A_g{}^b$ and $A_g{}^t$, are expected to be maximally enhanced by the dominant A term RR scattering mechanism,[36] the degree of enhancement depending on the Franck–Condon factors. The Franck–Condon factor for the bridge breathing mode appears to maximize at the deepest blue transition for Ado, but at a yellow transition for RPP, with Fd showing an intermediate pattern. The terminal $A_g{}^t$ mode is maximally enhanced in the green and yellow region for both Fd (339-cm^{-1} band) and RPP (336 cm^{-1}). In the case of Ado, however, this band (329 cm^{-1}) is surprisingly weak at all of the wavelengths, whereas the $B_{3u}{}^b$ mode at 349 cm^{-1} becomes the strongest one in the spectrum with 530.9-nm excitation.

(36) Spiro, T. G.; Stein, P. *Annu. Rev. Phys. Chem.* **1977**, *28*, 501–521.

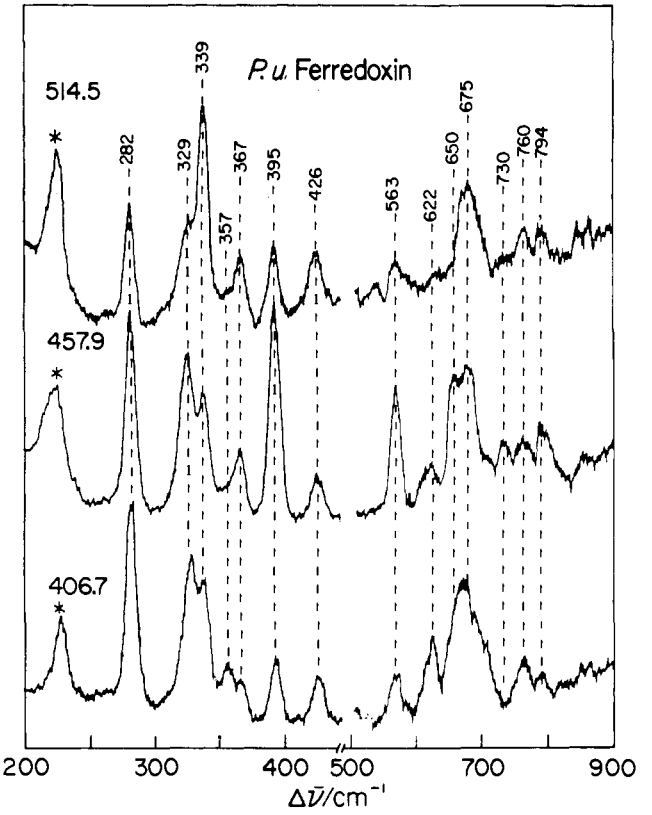

Figure 6. Resonance Raman spectra (77 K) of *P. umbilicalis* Fd excited at 406.7, 457.9, and 514.5 nm. All the spectra were obtained from the same sample so that the ice band (*) can be used as an internal standard. The intensity scale of the high-frequency region is expanded ~3 times relative to the low-frequency region. Conditions: slit widths, 5 cm^{-1} (low frequency) and 8 cm^{-1} (high frequency); 0.5-cm^{-1} increments.

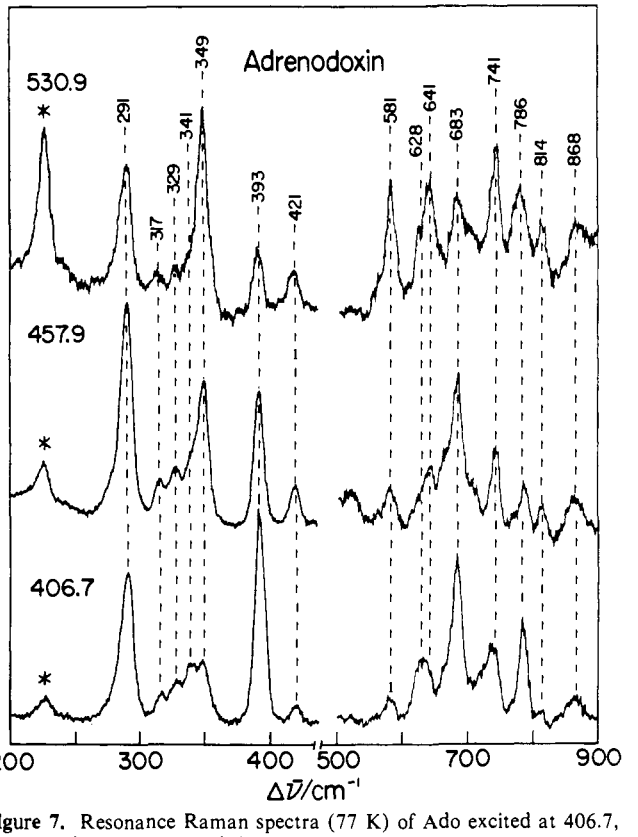

Figure 7. Resonance Raman spectra (77 K) of Ado excited at 406.7, 457.9, and 530.9 nm; conditions as in Figure 6.

Table V. Modeling of the Reduced Adrenodoxin Frequencies (cm^{-1})

adrenodoxin			$Fe_2S_2(SCH_3)_4$									mode	
oxidized[a]	reduced[a]	Δ[d]	oxidized[b]	PED[c]		reduced[b]	PED[c]				Δ[d]	D_{2h}	C_{2v}
421 (6.3)	398 (4.5)	23	412 (7.2)	b (80)		391 (6.6)	b (61)		b′ (18)		21	$B_{2u}{}^b$	B_1
393 (5.7)	377 (4.5)	16	390 (5.9)	b (80)	t (17)	374 (5.1)	b (64)	t (21)	b′ (7)	t′ (1)	16	$A_g{}^b$	A_1
349 (3.2)	307 (?)	42	346 (2.9)	b (50)	t (39)	314 (3.9)	b (1)	t (49)	b′ (30)	t′ (1)	32	$B_{3u}{}^b$	A_1
			326 (0.0)		t (86)	325 (0.1)		t (87)			1	$B_{1u}{}^t$	B_2
341 (0.8)	307 (?)	34	324 (0.0)		t (88)	274 (0.1)				t′ (80)	50	$B_{2g}{}^t$	B_2
329 (1.5)	307 (?)	22	321 (3.3)	b (19)	t (55)	302 (2.4)	b (13)	t (4)	b′ (23)	t′ (36)	19	$A_g{}^t$	A_1
317 (3.2)	276 (2.5)	41	309 (4.0)	b (53)	t (35)	276 (3.2)	b (27)		b′(60)		33	$B_{1g}{}^b$	B_1
291 (3.3)	276 (2.5)	15	279 (3.3)	b (31)	t (53)	258 (3.0)	b (6)	t (11)	b′ (21)	t′ (39)	21	$B_{3u}{}^t$	A_1

[a] Observed frequencies (cm^{-1}) and $^{34}S^b$ isotope shifts in parentheses. [b] Calculated frequencies (cm^{-1}) and $^{34}S^b$ isotope shifts in parentheses for a D_{2h} model (oxidized) with the same force field and geometry as the S_2-o-xyl calculation,[21] except point mass (15 amu) CH_3 groups replaced the CH_2CH_3 groups. The reduced protein frequencies were calculated with a C_{2v} model having $K(Fe^{II}\text{–}S)/K(Fe^{III}\text{–}S) = 0.7$ but the same geometry. [c] Calculated potential energy distribution (%): b = $Fe^{III}\text{–}S^b$; t = $Fe^{III}\text{–}S^t$; b′ = $Fe^{II}\text{–}S^b$; t′ = $Fe^{II}\text{–}S^t$. [d] Downshifts upon reduction, i.e., ν(oxidized) − ν(reduced).

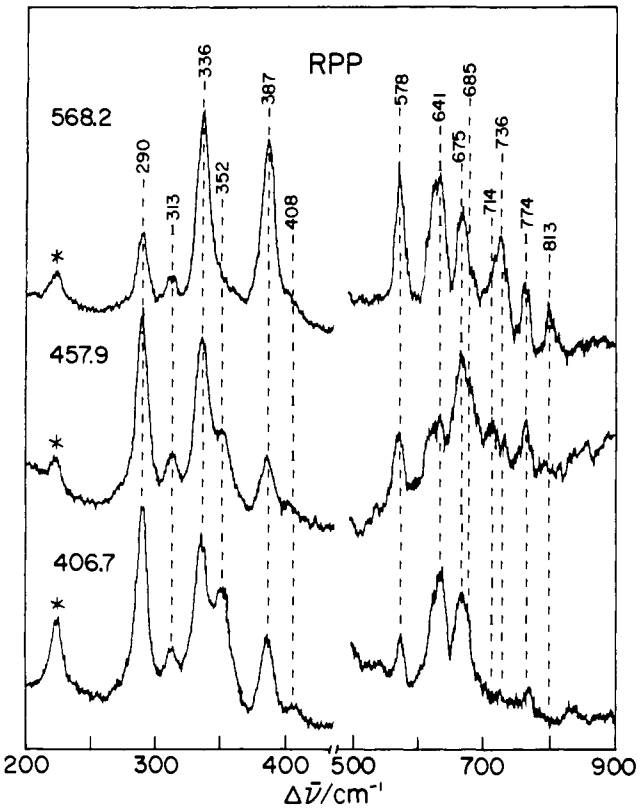

Figure 8. Resonance Raman spectra (77 K) of *C. pastuerianum* RPP excited at 406.7, 457.9, and 568.2 nm; conditions as in Figure 6.

Another striking feature, seen for all three proteins, is the large cross section, at most wavelengths, for the other B_{3u} band, $B_{3u}{}^t$ at 282, 291, and 290 cm^{-1} for Fd, Ado, and RPP, respectively. The RR intensity of this infrared mode has been noted earlier.[13] For all the infrared modes, RR enhancement is attributable to loss of the symmetry center of the chromophore due to an asymmetric environment in the protein. As discussed in the preceding paper,[21] the nature of the $B_{3u}{}^t$ mode makes it particularly susceptible to environmental influences. Its eigenvector describes a concerted out-of-phase breathing motion of the linked FeS_4 tetrahedra (see Figure 10 of ref 21). This mode would be expected to have a large Raman polarizability were it not for the phase cancellation of the two tetrahedra; this cancellation would be removed by an asymmetric environment. The $B_{3u}{}^t$ and $B_{3u}{}^b$ modes are polarized along the Fe–Fe axis, and the likeliest asymmetric perturbation would be differential H-bonding to the terminal cysteine sulfur atoms. As noted earlier[31], the *S. platensis* Fd crystal structure shows this kind of asymmetry. The cysteine S atoms on one side of the cluster have two H bonds each, while those on the other side have zero and one H bond. Similar asymmetry is implied for all three proteins by the $B_{3u}{}^t$ band intensity.

Also shown in Figures 6–8 is the overtone and combination region of the Fe–S stretches. Assignments of these bands are indicated in Table IV. To a first approximation, the intensities of the overtones and combinations should be proportional to the squares and products of intensities of the corresponding fundamentals.[37] Deviations from various expectations are attributable to higher order effects involving changes in the excited-state force constants and normal mode compositions (Duschinsky rotation).[38] Appreciable effects of this sort can be seen in the overtone intensity pattern. For example, in the 457.9-nm excited Fd spectrum, the 395-cm^{-1} $A_g{}^b$ band is stronger than the 339-cm^{-1} $A_g{}^t$ band, but the overtone of the latter is much stronger than that of the former. Likewise, in the 530.9-nm excited Ado spectrum, the overtone of the strongest band, $B_{3u}{}^b$ at 349 cm^{-1}, is scarcely discernible at 698 cm^{-1}, whereas its 741-cm^{-1} combination with the weaker $A_g{}^b$ band at 393 cm^{-1} is strong. We are unable to identify a C–S stretching mode of the cysteine ligands in the spectra. This mode was tentatively assigned to a 653-cm^{-1} band in rubredoxin RR spectra,[39] a position that is obscured for the Fe_2S_2 proteins by the $B_{3u}{}^t + B_{3u}{}^b$ combination.

4. Reduced Adrenodoxin and RPP. All attempts to obtain RR spectra of reduced Fd failed, but good quality spectra of reduced Ado[13,19] and RPP can be obtained with yellow excitation[40] as shown in Figure 9. This protein variability can be related to the prominent long wavelength absorption bands of reduced Ado and RPP at 540 and 552 nm, respectively (see Figure 4). Fd shows only weak featureless absorption in this spectral region. The CT transitions responsible for the RR enhancement in reduced Ado or RPP must be shifted or weakened in Fd. The RR spectra of reduced Ado and RPP are quite similar. The Ado $^{34}S^b$ isotope shifts permit correlations of the 398- and 377-cm^{-1} features with the bridging modes seen at 421 and 393 cm^{-1} in the oxidized protein. Assignment of the broad 307- and 276-cm^{-1} bands is less certain, but the weak isotope shifts imply major involvement of the terminal stretches.

We have modeled the reduced RR spectrum with the calculation given in Table V. As before,[21] a methanethiolate analogue model was used, with the structural parameters of the $[Fe_2S_2(S_2\text{-o-xyl})_2]^{2-}$ complex.[35] The force field developed in the preceding study[21] for the analogue spectra was utilized, but the symmetry was reduced to C_{2v}, allowing for inequivalent Fe–S bonds. The principal Fe–S stretching force constants were lowered for one of the two Fe atoms, to allow for the bond weakening expected for Fe^{II} relative to Fe^{III}. It is known that the added electron is localized on one end of the complex[2] (probably the end with the larger number

(37) (a) Heller, E. J. *Acc. Chem. Res.* **1981**, *14*, 368. (b) Heller, E. J.; Sundberg, R. L. *J. Phys. Chem.* **1982**, *86*, 1822.

(38) Blair, D. F.; Campbell, G. W.; Schoonover, J. R.; Chan, S. I.; Gray, H. B.; Malmstrom, B. G.; Pecht, I.; Swanson, B. I.; Woodruff, W. H.; Cho, W. K.; English, A. M.; Fry, H. A.; Lum, V.; Norton, K. A. *J. Am. Chem. Soc.* **1985**, *107*, 3755.

(39) Czernuszewicz, R. S.; LeGall, J.; Moura, I.; Spiro, T. G. *Inorg. Chem.* **1986**, *25*, 696–700.

(40) The RR spectrum of reduced RPP was also produced with 413.1-nm excitation although the resonance enhancement was much weaker than with 568.2-nm excitation.

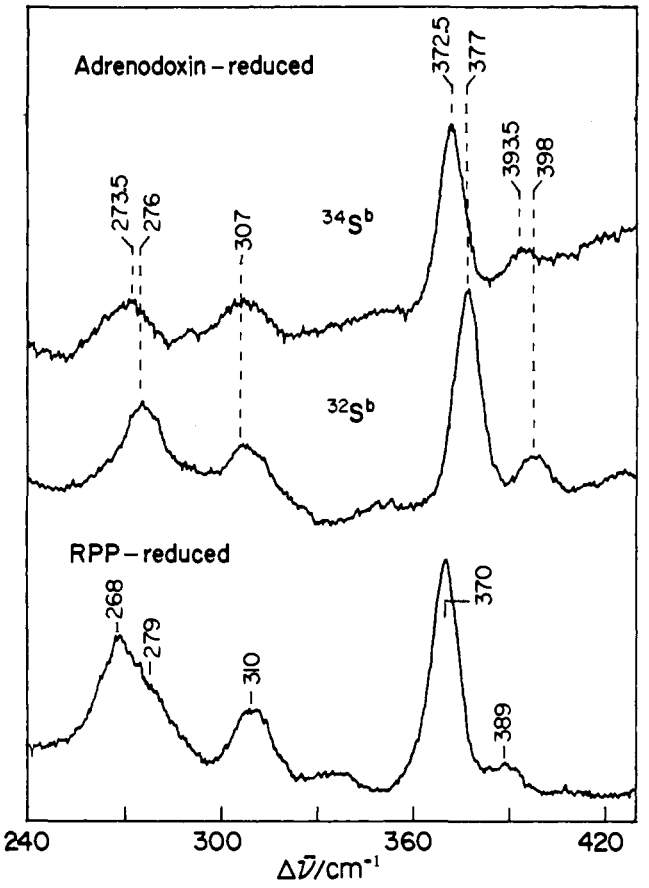

Figure 9. Resonance Raman spectra (77 K) of reduced Ado and *C. pastuerianum* RPP obtained with 530.9- and 568.2-nm excitations, respectively, and 6-cm^{-1} slit widths (0.5-cm^{-1} increments).

of H bonds to the cysteine S atoms). As seen in Table V, good results were obtained with a $K(Fe^{II}-S)/K(Fe^{III}-S)$ force constant ratio of 0.7. The high-frequency bridging modes, $B_{2u}{}^b$ (421 cm^{-1}) and $A_g{}^b$ (393 cm^{-1}) shift down by the observed intervals, and the remaining bands are calculated to group together so that their overlapping contributions could easily account for the broad 307- and 276-cm^{-1} features. Since the electronic transition providing the resonance enhancement is undoubtedly a $S \rightarrow Fe^{III}$ CT transition, it is reasonable to assume that most of the RR intensity is associated with coordinates centered on the Fe^{III} side of the complex. Indeed, the calculated potential energy distribution (Table V) does give a rough guide to the RR intensities, and it is not surprising that the 377-cm^{-1} band is the strongest one in the reduced spectrum, since it involves bonds to the Fe^{III} almost exclusively. On the other hand, the strong 291-cm^{-1} band in the oxidized Ado spectrum, $B_{3u}{}^t$, correlates with a band which is mainly Fe^{II}–S stretching in character, calculated to fall at 258 cm^{-1} in the reduced spectrum. Failure to observe this band can be attributed to its Fe^{II}–S character.

Conclusions

RR spectra have been assigned for the major classes of Fe_2S_2 proteins. All of the Fe–S stretching bands are activated, including the infrared bands which are inactive in analogue RR spectra. This activation implies an asymmetric protein environment, suggested to be due to differential H-bonding to the cysteine S atoms on the two ends of the complex. Strong activation of the ~290-cm^{-1} $B_{3u}{}^t$ mode is attributable to its out-of-phase breathing character. The frequencies of corresponding bands vary appreciably among the three proteins and the analogue complexes. This variation is attributed to increased bridging and terminal Fe–S bond strengths in the protein relative to the analogues, due to protein compression effects or to stabilizing H-bond interactions which ameliorate the negative charge on the complex. In addition there is evidence in Fd for Fe–S–C–C dihedral angles somewhat greater than 90°, allowing mixing of the S–C–C bending coordinates with the terminal Fe–S stretches. Pronounced differences are also seen in the RR enhancement patterns, indicating that the resonant $S \rightarrow Fe$ CT transitions are altered by the structural variations. RR spectra of reduced Ado and RPP are in accord with a localized model in which the Fe–S bond strength is reduced by ~30% upon reduction and enhancement is provided by the CT transitions to the unreduced Fe.

Acknowledgment. This work was supported by NIH Grant GM13498 (to T.G.S.).

Novel Cytotoxic and Phytotoxic Halogenated Sesquiterpenes from the Green Alga *Neomeris annulata*[1]

David E. Barnekow,[†] John H. Cardellina, II,*[,†] Andrew S. Zektzer,[‡,2] and Gary E. Martin[‡]

Contribution from the Natural Products Laboratory, Department of Chemistry, Montana State University, Bozeman, Montana 59717, and Department of Medicinal Chemistry, College of Pharmacy, University of Houston, Houston, Texas 77004. *Received June 13, 1988*

Abstract: The cytotoxicity and phytotoxicity observed in extracts of the calcareous green alga *Neomeris annulata* were traced to a fraction containing a trio of new halogenated sesquiterpenes. The application of zero-quantum and reverse-detected multiple-quantum 2D NMR techniques was pivotal in the elucidation of the structures. Three different, seemingly biosynthetically related carbon skeletons, one of them (neomeranol) unprecedented, are represented by these constitutional isomers. While a few halogenated phenols and quinones are known from green algae, this is the initial discovery of halogenated sesquiterpenes in the Chlorophyta.

Neomeris annulata is a diminutive calcareous green alga widely distributed in the shallow, inshore waters of Bermuda. The organic soluble extracts of collections made in 1984 and 1986 exhibited phytotoxicity to johnsongrass, brine shrimp toxicity, and marginal cytotoxicity (KB: ED_{50} 29 μg/mL) in our pharmacological/agrochemical screening program. Bioassay guided fractionation traced the activities observed to a trio of new monobrominated sesquiterpene alcohols. This is the first report of halogenated sesquiterpenes from a green alga and the first association of

[†] Montana State University.
[‡] University of Houston.

(1) Contribution No. 1123 from the Bermuda Biological Station and from the Montana Agricultural Experiment Station.
(2) Current address: Abbott Laboratories, N. Chicago, IL.

0002-7863/89/1511-3511$01.50/0